Bismuth Flux Growth of $CeRh_6Ge_4$ and $CeRh_2Ge_2$ Single Crystals

Daniel Voßwinkel, Oliver Niehaus, Ute Ch. Rodewald, and Rainer Pöttgen

Institut für Anorganische und Analytische Chemie, Universität Münster, Corrensstrasse 30, 48149 Münster, Germany

Reprint requests to R. Pöttgen. E-mail: pottgen@uni-muenster.de

Z. Naturforsch. **2012**, *67b*, 1241 – 1247 / DOI: 10.5560/ZNB.2012-0265
Received October 4, 2012

Single crystals of the germanides $CeRh_6Ge_4$ and $CeRh_2Ge_2$ were synthesized from the elements in bismuth fluxes. Polycrystalline samples are available by arc-melting. The structures were refined on the basis of single-crystal X-ray diffractometer data. $CeRh_6Ge_4$: $LiCo_6P_4$ type, $P\bar{6}m2$, $a = 715.4(2)$, $c = 385.5(1)$ pm, $wR2 = 0.0554$, 273 F^2 values, 19 variables; $CeRh_2Ge_2$: $ThCr_2Si_2$ type, $I4/mmm$, $a = 415.69(6)$, $c = 1048.5(2)$ pm, $wR2 = 0.0391$, 131 F^2 values, 9 variables. The rhodium and germanium atoms build three-dimensional, covalently bonded $[Rh_6Ge_4]$ and $[Rh_2Ge_2]$ networks with Rh–Ge distances ranging from 246 to 255 pm. The cerium atoms are located in larger cavities within these networks: $Ce@Ge_6Rh_{12}$ in $CeRh_6Ge_4$ and $Ce@Ge_8Rh_8$ in $CeRh_2Ge_2$. Temperature-dependent magnetic susceptibility data of $CeRh_6Ge_4$ show Curie-Weiss behavior above 70 K with an experimental magnetic moment of 2.35(1) μ_B per Ce atom. Low-field measurements are indicative of magnetic ordering below 2.5 K.

Key words: Bismuth Flux, Crystal Structure, Cerium, Germanide, Magnetism

Introduction

The ternary phase diagram Ce-Rh-Ge has been studied in detail by Shapiev [1]. Based on metallographic analyses in comparison with powder X-ray diffraction, twenty ternary germanides were detected. So far, only for half of these phases the structures are known, and furthermore, superstructure formation or phase transitions exist for some of these germanides. The standard procedure for the preparation of such germanides is arc-melting and subsequent annealing. In several cases the phases can be synthesized in polycrystalline form, however, often no single crystals suitable for structure refinement are obtained.

In recent years we studied the crystal chemistry and magnetic properties of the equiatomic germanide CeRhGe [2, 3] which orders antiferromagnetically at 9.3 K [4 – 9]. Orientation-dependent susceptibility studies of a single crystal [8] showed a phase transition at around 510 K which is subjected to a hysteresis. X-Ray powder diffraction data in the same temperature range showed a pronounced increase of the unit cell volume and an increase of the *c* parameter / decrease of the *a* parameter, both by about 30 pm [10]. In order to understand these drastic changes in the structure in more detail, we performed new crystal growth experiments. Since the standard techniques did not result in well-shaped crystals we decided to work with a metal flux [11, 12]. Bismuth was used as flux agent, and first experiments resulted in well-shaped crystals of $CeRh_2Ge_2$ ($ThCr_2Si_2$ type) and $CeRh_6Ge_4$ ($LiCo_6P_4$ type). The structure refinements of both germanides are reported herein. So far, only powder X-ray and neutron diffraction data have been published for $CeRh_2Ge_2$ [13 – 21]. The germanide $CeRh_6Ge_4$ (9.1 at.-% Ce : 54.5 at.-% Rh : 36.4 at.-% Ge) most likely corresponds to the phase with the approximate composition '$CeRh_5Ge_3$' (11.1 : 55.5 : 33.3) reported for the Ce-Rh-Ge phase diagram by Shapiev [1].

Experimental

Synthesis

Starting materials for the syntheses of the $CeRh_6Ge_4$ and $CeRh_2Ge_2$ samples were sublimed cerium pieces (Johnson Matthey), rhodium powder (Heraeus), germanium pieces (Chempur), and elongated bismuth shots (ABCR), all with stated purities better than 99.9 %. Polycrystalline samples have become available directly *via* arc-melting [22] of the elements under an argon atmosphere of *ca.* 700 mbar. The

argon was purified over titanium sponge (900 K), silica gel, and molecular sieves. In the case of $CeRh_6Ge_4$, the sample showed weak reflections of a (not yet identified) by-product. The sample was crushed, pressed to a pellet and arc-melted again. The by-product disappeared after this re-melting procedure. Single crystals were grown from bismuth fluxes. A Ce : Rh : Ge : Bi starting composition of 1 : 2 : 2 : 25 was used for the growth of $CeRh_2Ge_2$ crystals. The elements were sealed in an evacuated silica ampoule and heated within 2 h to 1320 K in a muffle furnace. The temperature was kept for one hour, followed by cooling at a rate of 8 K h^{-1} to 570 K and subsequently at 2 K h^{-1} to 530 K. Finally the tube was cooled to room temperature by switching off the furnace. The starting composition was 1 : 5 : 4 : 50 for the synthesis of $CeRh_6Ge_4$. Again, the tube was heated to 1320 K within 2 h, kept at 1320 K for 4 h, followed by slow cooling at a rate of 6 K h^{-1} to 770 K and then at 7 K h^{-1} to 520 K. After the last cooling step, the tube was cooled to room temperature by switching off the furnace. The bismuth flux was then dissolved in a 1 : 1 molar mixture of H_2O_2 (ACROS, 35 %) and glacial acetic acid (VWR International). The resulting $CeRh_6Ge_4$ and $CeRh_2Ge_2$ crystals are stable over months.

EDX data

Semiquantitative EDX analyses of the single crystals studied on the diffractometer were carried out in variable pressure mode with a Zeiss EVO® MA10 scanning electron microscope with CeO_2, Rh, and Ge as standards. The experimentally observed average compositions (9±1 at.-% Ce : 57±2 at.-% Rh : 34±2 at.-% Ge for the $CeRh_6Ge_4$ crystal and 20±1 at.-% Ce : 43±2 at.-% Rh : 37±2 at.-% Ge for the $CeRh_2Ge_2$ crystal) were close to the ideal ones. No impurity elements (especially residual bismuth from the flux) were detected. $CeRh_6Ge_4$ crystallizes in the form of pillars with a characteristic shape of the tail (Fig. 1), similar to the structurally closely related phosphide $ScRh_6P_4$ [23].

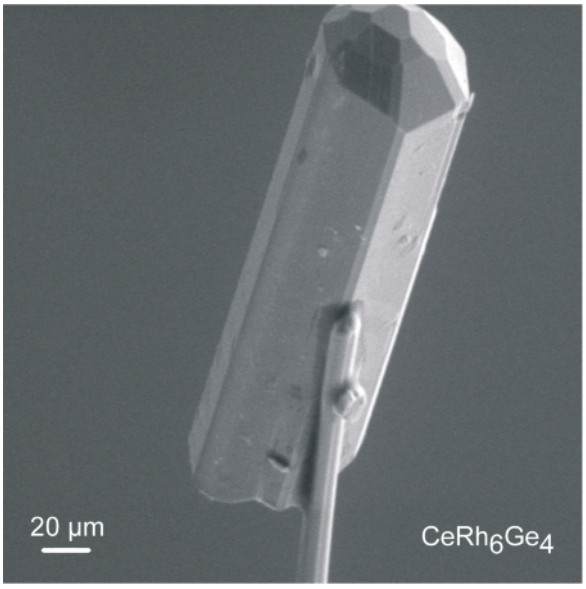

Fig. 1. A single crystal of $CeRh_6Ge_4$ mounted on a quartz fiber. The white bar at the lower left-hand side corresponds to 20 μm.

X-Ray diffraction

The polycrystalline and single-crystalline $CeRh_6Ge_4$ and $CeRh_2Ge_2$ samples were characterized by Guinier patterns

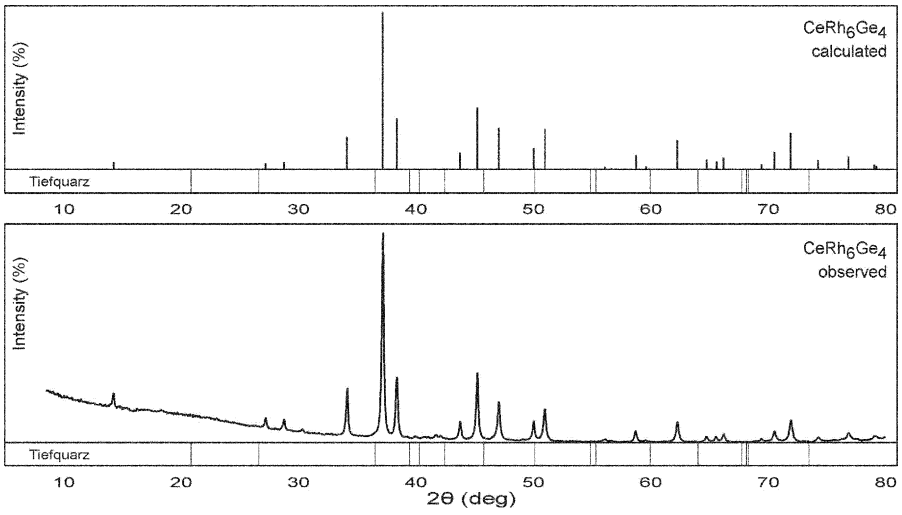

Fig. 2. Experimental and simulated Guinier powder pattern (Cu $K_{\alpha 1}$ radiation) of $CeRh_6Ge_4$.

Table 1. Crystal data and structure refinement for $CeRh_6Ge_4$ and $CeRh_2Ge_2$.

Empirical formula	$CeRh_6Ge_4$	$CeRh_2Ge_2$
Formula weight, g mol^{-1}	1047.94	491.12
Unit cell dimension (Guinier powder data)		
a, pm	715.4(2)	415.91(6)
c, pm	385.5(1)	1048.5(2)
Cell volume V, nm^3	0.1709	0.1812
Space group; Z	$P\bar{6}m2$; 1	$I4/mmm$; 2
Calculated density, g cm^{-3}	10.18	9.00
Crystal size, μm^3	$70 \times 70 \times 160$	$30 \times 60 \times 60$
Transmission ratio (min / max)	0.070 / 0.280	0.367 / 0.864
Absorption coefficient, mm^{-1}	37.8	37.4
$F(000)$, e	456	424
θ range for data collection, deg	3 – 33	5 – 34
Range in hkl	±10, ±10, ±5	±6, ±6, ±15
Total no. of reflections	3978	1244
Independent reflections / R_{int}	273 / 0.0389	131 / 0.0430
Reflections with $I > 2\,\sigma(I)$ / R_σ	271 / 0.0113	88 / 0.0369
Data / parameters	273 / 19	131 / 9
Goodness-of-fit on F^2	1.244	0.842
$R1$ / $wR2$ for $I > 2\,\sigma(I)$	0.0236 / 0.0554	0.0192 / 0.0387
$R1$ / $wR2$ for all data	0.0237 / 0.0554	0.0246 / 0.0391
Extinction coefficient	0.23(1)	0.0045(6)
BASF	0.51(3)	–
Largest diff. peak / hole, e Å^{-3}	3.30 / −1.90	1.79 / −0.94

(imaging plate detector, Fujifilm BAS-1800) with Cu $K_{\alpha1}$ radiation and α-quartz ($a = 491.30$, $c = 540.46$ pm) as an internal standard. For preparation of the samples for powder diffraction, both products were carefully crushed in a hardened steel mortar and subsequently ground with a small amount of *n*-hexane in an agate mortar. The lattice parameters (Table 1) were deduced from a standard least-squares procedure. Correct indexing of the patterns was ensured through intensity calculations [24]. For $CeRh_2Ge_2$ our data compared well with the original work by Venturini and Malaman of $a = 415.0(1)$ and $c = 1046.8(3)$ pm [16]. The experimental and calculated powder patterns of the $CeRh_6Ge_4$ sample are presented in Fig. 2.

Well-shaped singe crystals were selected from the $CeRh_6Ge_4$ and $CeRh_2Ge_2$ samples, glued to quartz fibers using bees-wax and studied on a Buerger camera (using white Mo radiation) to check their quality. The data sets were measured on a Stoe Stadi Vari diffractometer equipped with a Mo micro focus source and a Pilatus detection system. Numerical absorption corrections were applied to the data sets. Details about the data collections and the crystallographic parameters are summarized in Table 1.

Structure refinements

The $CeRh_2Ge_2$ data set showed a body-centered tetragonal lattice and no further systematic extinctions in agreement with the powder neutron diffraction data [16]. Those atomic parameters were taken as starting values, and the structure was refined with anisotropic displacement parameters for all atoms with SHELXL-97 (full-matrix least-squares on F_o^2) [25]. A hexagonal lattice without further systematic extinction conditions was observed for the $CeRh_6Ge_4$ data set. The non-centrosymmetric space group $P\bar{6}m2$ was found to be correct during structure refinement. The starting atomic parameters were deduced from Direct Methods with SHELXS-97 [26], and the structure was refined with anisotropic displacement parameters for all atoms. Calculation of the Flack parameter [27, 28] indicated twinning by inversion. Subsequently the inversion twin matrix and a BASF were introduced, and the structure was refined again. To check for deviations from the ideal compositions, the occupancy parameters were refined in separate series of least-squares cycles for both data sets. All sites were fully occupied within two standard deviations. The final difference Fourier synthesis revealed no residual peaks. The refined atomic positions, equivalent isotropic displacement parameters, and interatomic distances are given in Tables 2 and 3.

Table 2. Atomic coordinates and equivalent isotropic displacement parameters (pm^2) for $CeRh_6Ge_4$ and $CeRh_2Ge_2$. U_{eq} is defined as one third of the trace of the orthogonalized U_{ij} tensor.

Atom	Site	x	y	z	U_{eq}
$CeRh_6Ge_4$ ($P\bar{6}m2$)					
Ce	1*a*	0	0	0	141(3)
Rh1	3*j*	0.53312(7)	$-x$	0	131(3)
Rh2	3*k*	0.20073(7)	$-x$	1/2	127(3)
Ge1	1*c*	1/3	2/3	0	128(4)
Ge2	3*k*	0.80144(10)	$-x$	1/2	141(3)
$CeRh_2Ge_2$ ($I4/mmm$)					
Ce	2*a*	0	0	0	163(3)
Rh	4*d*	0	1/2	1/4	157(2)
Ge	4*e*	0	0	0.37475(14)	164(3)

Table 3. Interatomic distances (pm), for $CeRh_6Ge_4$ and $CeRh_2Ge_2$ calculated with the powder lattice parameters. Standard deviations are equal or smaller than 0.2 pm. All distances of the first coordination spheres are listed.

$CeRh_6Ge_4$				$CeRh_2Ge_2$			
Ce:	6	Ge2	312.6	Ce:	8	Ge	321.9
	6	Rh2	314.7		8	Rh	334.5
	6	Rh1	360.1		2	Ge	392.9
	2	Ce	385.5		4	Ce	415.7
Rh1:	1	Ge1	247.6	Rh:	4	Ge	245.6
	4	Ge2	254.5		4	Rh	293.9
	2	Rh1	286.6		4	Ce	334.5
	4	Rh2	291.1	Ge:	4	Rh	245.6
	2	Ce	360.1		1	Ge	262.7
Rh2:	2	Ge2	247.4		4	Ce	321.9
	2	Ge1	253.3		1	Ce	392.9
	2	Rh2	284.6				
	4	Rh1	291.1				
	2	Ce	314.7				
Ge1:	3	Rh1	247.6				
	6	Rh2	253.3				
Ge2:	2	Rh2	247.4				
	4	Rh1	254.5				
	2	Ge2	289.3				
	2	Ce	312.6				

Further details of the crystal structure investigation may be obtained from Fachinformationszentrum Karlsruhe, 76344 Eggenstein-Leopoldshafen, Germany (fax: +49-7247-808-666; E-mail: crysdata@fiz-karlsruhe.de, http://www.fiz-karlsruhe.de/request_for_deposited_data.html) on quoting the deposition number CSD-425231 ($CeRh_6Ge_4$) and CSD-425230 ($CeRh_2Ge_2$).

Magnetic susceptibility measurements

Magnetic measurements were carried out on a Quantum Design Physical Property Measurement System using the VSM option. 17.881 mg of the $CeRh_6Ge_4$ sample was packed in kapton foil and attached to the sample holder rod. The measurements were performed in the temperature range of 2.5 – 300 K with magnetic flux densities up to 80 kOe.

Discussion

Crystal chemistry

Our recent synthetic work has shown that well-shaped crystals of ternary germanides can be grown from bismuth fluxes. This offers a new access to germanides. Especially in cases where only polycrystalline samples with unknown structures are available, crystal growth from a flux allows for a reliable structure determination. The two examples presented here show that bismuth acts as a non-reactive flux.

The single-crystal X-ray data obtained for $CeRh_2Ge_2$ ($ThCr_2Si_2$ type, *I*4/*mmm*) fully confirm the powder neutron diffraction experiments [16], but the germanium *z* parameter has been determined with higher precision herein. The crystal chemistry and chemical bonding of $ThCr_2Si_2$ phases has repeatedly been reviewed [29 – 32]. We therefore refer to the literature and turn to the discussion of the germanide $CeRh_6Ge_4$. This phase is not a new one. It most likely corresponds to the phase with the approximate composition '$CeRh_5Ge_3$' reported by Shapiev [1].

$CeRh_6Ge_4$ crystallizes with the hexagonal $LiCo_6P_4$-type [33] structure, space group $P\bar{6}m2$. This structure type has also been observed for the pnictides α-UCr_6P_4 [34], $MgCo_6P_4$ [35], $MgRh_6P_4$, $MgRh_6As_4$, $CaRh_6As_4$, $SrRh_6As_4$, and $YbRh_6As_4$ [36]. The phosphides $RERh_6P_4$ (*RE* = Sc, Yb, Lu) [23] adopt a superstructure of the $LiCo_6P_4$ type through two *translationengleiche* symmetry reductions. $CeRh_6Si_4$ [37] and $CeRh_6Ge_4$ are the first tetrelides that crystallize with this structure type. Interestingly, this structure type had also been observed for the chemically related compounds KIn_6Au_4 and $RbIn_6Au_4$ [38] which can be classified as aurides. This reverse type of transition metal-*p*-element ordering is a consequence of the trend in the electronegativities, Au and P being the most electronegative ones in $LiCo_6P_4$ and KIn_6Au_4, respectively. At first sight this seems strange, but such type/anti-type pairs frequently occur in intermetallic chemistry, *e. g.* $Hf_2Co_4P_3$ *vs.* $Sr_2In_4Au_3$ [39] or YCo_5P_3 *vs.* $Ca_2In_4Au_3$ [40].

A projection of the $CeRh_6Ge_4$ structure along the short unit cell axis is presented in Fig. 3. The rhodium and germanium atoms build up a three-dimensional $[Rh_6Ge_4]$ network in which the cerium atoms fill large hexagonal channels. The Rh–Ge distances range from 247 to 255 pm, close to the sum of the covalent radii [41] of 247 pm. They are also in the same range as in $CeRh_2Ge_2$ (Table 3). Each cerium atom in $CeRh_6Ge_4$ has six germanium and twelve rhodium neighbors. Along the channel that extends in *c* direction, two additional cerium neighbors are at Ce–Ce distances of 386 pm, well above the Hill limit [42] for *f* electron localization of 340 pm.

The cerium atoms in both $CeRh_6Ge_4$ and $CeRh_2Ge_2$ have six, respectively eight germanium atoms as nearest neighbors. This is different in the structure of equiatomic CeRhGe [2], where four short Ce–Rh distances in the range from 302 to 310 pm occur

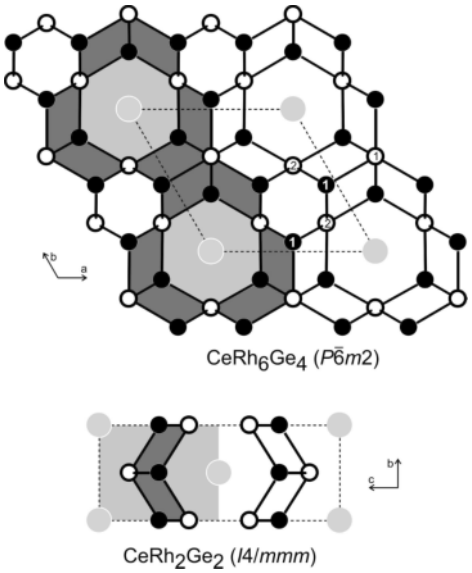

Fig. 3. Projection of the crystal structures of $CeRh_6Ge_4$ and $CeRh_2Ge_2$ along the short unit cell axis. Cerium, rhodium, and germanium atoms are drawn as light grey, black filled, and open circles, respectively. Similar structural slabs are shaded with medium and dark grey color.

in the first coordination shell. The Ce–Ge distances (312 – 313 pm), however, are in the same range.

The $[Rh_6Ge_4]$ network in $CeRh_6Ge_4$ shows also some Rh–Rh contacts. The Rh–Rh distances range from 285 to 291 pm, only slightly longer than in *fcc* rhodium (269 pm) [43]. Therefore the Rh–Rh contacts obviously also contribute to the stability of the network. In the structurally closely related phosphide $ScRh_6P_4$ [23] with the much smaller scandium atoms, the Rh–Rh distances of 278 – 293 pm are slightly shorter.

Although $CeRh_6Ge_4$ and $CeRh_2Ge_2$ have distinctly different composition, their structures are closely related, and one can describe the $CeRh_6Ge_4$ structure as an intergrowth of $CeRh_2Ge_2$ related slabs. The latter are shaded in Fig. 3. Three $CeRh_2Ge_2$-related slabs are rotated by 120° and packed together, leading to the hexagonal motif in $CeRh_6Ge_4$. Since three slabs share a common cerium atom, the Ce : Rh ratio increases from 1 : 2 to 1 : 6.

Magnetic properties of $CeRh_6Ge_4$

The temperature dependence of the susceptibility and inverse susceptibility (χ and χ^{-1} data), measured at an applied field of 10 kOe, is displayed in Fig. 4.

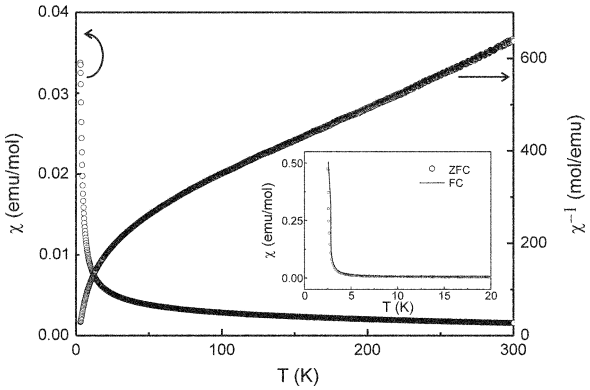

Fig. 4. Temperature dependence of the magnetic susceptibility (χ and χ^{-1} data) of $CeRh_6Ge_4$ measured at an applied field of 10 kOe. The low-temperature behavior in zero-field-cooled/field-cooled mode with an applied field of 100 Oe is depicted in the inset.

The inset shows the measurement in the zero-field-cooled/field-cooled (ZFC/FC) mode at an applied field of 100 Oe.

We were able to fit the inverse susceptibility data with the Curie-Weiss law in the temperature range of 70 to 300 K which yielded an effective magnetic moment of $\mu_{\mathrm{eff}} = 2.35(1)\ \mu_B$ per Ce atom, close to the range of experimental values for Ce^{3+} (2.3 – 2.5 μ_B per Ce atom). The moment is slightly smaller than the theoretical value of 2.54 μ_B for a free Ce^{3+} ion. Below 70 K we observed deviations from Curie-Weiss behavior due to splitting of the $J = 5/2$ ground state of Ce^{3+} and/or the onset of short-range magnetic interactions.

The sharp increase of the susceptibility at around 2.5 K (the lowest available temperature in our ex-

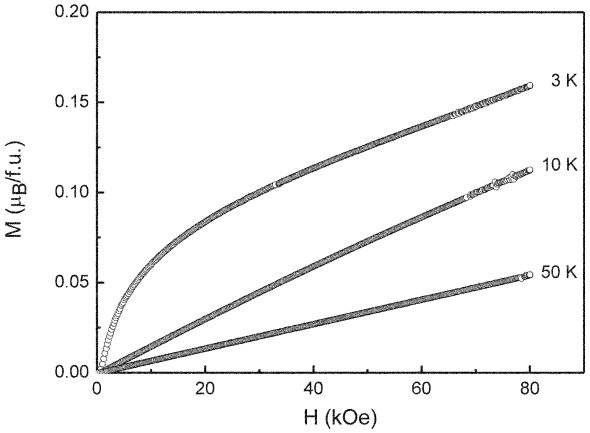

Fig. 5. Magnetization isotherms of $CeRh_6Ge_4$ measured at 3, 10 and 50 K.

perimental setup) in both the ZFC- and FC-data strongly hints towards magnetic ordering. Magnetization isotherms were measured at 3, 10, and 50 K up to 80 kOe (Fig. 5). Well above the possible magnetic ordering temperature, at 10 and 50 K, we observed a linear increase of the magnetization with increasing field as expected for a paramagnetic material. At 3 K the isotherm shows a curvature which is caused by the onset of magnetic ordering and/or saturation effects in a paramagnetic material. The magnetization at 3 K and 80 kOe is $\mu = 0.16(5)\ \mu_B$ per Ce atom, much lower than the expected value of 2.14 μ_B for Ce^{3+} (according to $g_J \times J$).

Conclusion

Bismuth is a suitable non-reactive flux medium for the growth of well-shaped germanide single crystals. The structures of $CeRh_6Ge_4$ (the first $LiCo_6P_4$-type germanide) and $CeRh_2Ge_2$ were refined on the basis of singe-crystal X-ray data. $CeRh_6Ge_4$ is an intergrowth variant of $CeRh_2Ge_2$.

Acknowledgement

This work was supported by the Deutsche Forschungsgemeinschaft. O. N. is indebted to the *NRW Research School Molecules and Materials* for a PhD stipend.

[1] B. I. Shapiev, Dissertation, Moscow State University, Moscow, **1993**.
[2] E. Gaudin, B. Chevalier, B. Heying, U. C. Rodewald, R. Pöttgen, *Chem. Mater.* **2005**, *17*, 2693.
[3] S. F. Matar, E. Gaudin, B. Chevalier, R. Pöttgen, *Solid State Sci.* **2007**, *9*, 274.
[4] P. Rogl, B. Chevalier, M. J. Besnus, J. Etourneau, *J. Magn. Magn. Mater.* **1989**, *80*, 305.
[5] B. Chevalier, P. Rogl, J. Etourneau, M. J. Besnus, *J. Magn. Magn. Mater.* **1990**, *83*, 303.
[6] B. Chevalier, P. Rogl, E. K. Hlil, M. H. Tuilier, P. Dordor, J. Etourneau, *Z. Phys. B* **1991**, *84*, 205.
[7] W. Bazela, A. Zygmunt, A. Szytuła, E. Ressouche, J. Leciejewicz, W. Sikora, *J. Alloys Compd.* **1996**, *243*, 106.
[8] T. Ueda, D. Honda, T. Shiromoto, N. Metoki, F. Honda, K. Kaneko, Y. Haga, T. D. Matsuda, T. Takeuchi, A. Thamizhavel, K. Sugiyama, K. Kindo, R. Settai, Y. Ônuki, *J. Phys. Soc. Jpn.* **2005**, *74*, 2836.
[9] T. Ueda, D. Honda, K. Sugiyama, T. Matsuda, N. Metoki, F. Honda, K. Kaneko, Y. Haga, T. Takeuchi, K. Kindo, R. Settai, Y. Ônuki, *Physica B* **2005**, *359–361*, 133.
[10] W. Hermes, R.-D. Hoffmann, B. Chevalier, R. Pöttgen, unpublished results.
[11] P. C. Canfield, Z. Fisk, *Phil. Mag B* **1992**, *65*, 1117.
[12] M. G. Kanatzidis, R. Pöttgen, W. Jeitschko, *Angew. Chem. Int. Ed.* **2005**, *44*, 6996.
[13] M. Francois, G. Venturini, J. F. Marêché, B. Malaman, B. Roques, *J. Less-Common Met.* **1985**, *113*, 231.
[14] I. Felner, I. Nowik, *J. Phys. Chem. Solids* **1985**, *46*, 681.
[15] G. Venturini, B. Malaman, *Solid State Commun.* **1988**, *66*, 597.
[16] G. Venturini, B. Malaman, *Solid State Commun.* **1988**, *67*, 193.
[17] J. D. Thompson, Y. Uwatoko, T. Graf, M. F. Hundley, D. Mandrus, C. Godart, L. C. Gupta, P. C. Canfield, A. Migliori, H. A. Borges, *Physica B* **1994**, *199&200*, 589.
[18] Y. Uwatoko, G. Oomi, T. Graf, J. D. Thompson, P. C. Canfield, H. A. Borges, C. Godart, L. C. Gupta, *Physica B* **1995**, *206&207*, 234.
[19] T. Ooshima, M. Ishikawa, *J. Phys. Soc. Jpn.* **1998**, *67*, 3251.
[20] H. Abe, K. Yoshii, H. Kitazawa, *Physica B* **2002**, *312–313*, 253.
[21] H. Kadowaki, T. Fukuhara, K. Maezawa, N. Aso, H. Yoshizawa, T. Ooshima, M. Ishikawa, *J. Phys. Soc. Jpn.* **2002**, *71*, 2069.
[22] R. Pöttgen, Th. Gulden, A. Simon, *GIT Labor-Fachzeitschrift* **1999**, *43*, 133.
[23] U. Pfannenschmidt, U. Ch. Rodewald, R. Pöttgen, *Monatsh. Chem.* **2011**, *142*, 219.
[24] K. Yvon, W. Jeitschko, E. Parthé, *J. Appl. Crystallogr.* **1977**, *10*, 73.
[25] G. M. Sheldrick, SHELXL-97, Program for the Refinement of Crystal Structures, University of Göttingen, Göttingen (Germany) **1997**. See also: G. M. Sheldrick, *Acta Crystallogr.* **2008**, *A64*, 112.
[26] G. M. Sheldrick, SHELXS-97, Program for the Solution of Crystal Structures, University of Göttingen, Göttingen (Germany) **1997**. See also: G. M. Sheldrick, *Acta Crystallogr.* **1990**, *A46*, 467.
[27] H. D. Flack, G. Bernadinelli, *Acta Crystallogr.* **1999**, *A55*, 908.
[28] H. D. Flack, G. Bernadinelli, *J. Appl. Crystallogr.* **2000**, *33*, 1143.
[29] D. Kußmann, R. Pöttgen, U.Ch. Rodewald, C. Rosenhahn, B. D. Mosel, G. Kotzyba, B. Künnen, *Z. Naturforsch.* **1999**, *54b*, 1155.

[30] E. Parthé, L. Gelato, B. Chabot, M. Penzo, K. Cenzual, R. Gladyshevskii, TYPIX-Standardized Data and Crystal Chemical Characterization of Inorganic Structure Types, *Gmelin Handbook of Inorganic and Organometallic Chemistry*, 8th edition, Springer, Berlin **1993**.
[31] C. Zheng, R. Hoffmann, *J. Solid State Chem.* **1988**, *72*, 58.
[32] D. Johrendt, C. Felser, O. Jepsen, O. K. Andersen, A. Mewis, J. Rouxel, *J. Solid State Chem.* **1997**, *130*, 254.
[33] R. Buschmann, H.-U. Schuster, *Z. Naturforsch.* **1991**, *46b*, 699.
[34] W. Jeitschko, R. Brink, *Z. Naturforsch.* **1992**, *47b*, 192.
[35] A. Hellmann, A. Mewis, *Z. Anorg. Allg. Chem.* **2001**, *627*, 1357.
[36] A. Wurth, A. Mewis, *Z. Anorg. Allg. Chem.* **1999**, *625*, 449.
[37] A. Lipatov, A. Gribanov, A. Grytsiv, S. Safronov, P. Rogl, J. Rousnyak, Y. Seropegin, G. Giester, *J. Solid State Chem.* **2010**, *183*, 829.
[38] B. Li, J. D. Corbett, *Inorg. Chem.* **2007**, *46*, 6022.
[39] R.-D. Hoffmann, R. Pöttgen, C. Rosenhahn, B. D. Mosel, B. Künnen, G. Kotzyba, *J. Solid State Chem.* **1999**, *145*, 283.
[40] R.-D. Hoffmann, R. Pöttgen, *Z. Anorg. Allg. Chem.* **1999**, *625*, 994.
[41] J. Emsley, *The Elements*, Oxford University Press, Oxford **1999**.
[42] H. H. Hill in *Plutonium and other Actinides*, (Ed.: W. N. Mines), Nuclear Materials Series, AIME, **1970**, *17*, 2.
[43] J. Donohue, *The Structures of the Elements*, Wiley, New York **1974**.